41. CRUSTAL ACCRETION IN THE GULF OF CALIFORNIA: AN INTERMEDIATE-RATE SPREADING AXIS[1]

Paul T. Robinson, Department of Geology, Dalhousie University, Halifax, Nova Scotia, Canada
Brian T. R. Lewis, Department of Oceanography, University of Washington, Seattle, Washington
Martin F. J. Flower, Department of Geological Sciences, University of Illinois at Chicago Circle, Chicago, Illinois
Matthew H. Salisbury, Geologic Research Division, Scripps Institution of Oceanography, La Jolla, California
and
Hans-Ulrich Schmincke, Institut für Mineralogie, Ruhr-Universität Bochum, Bochum, West Germany

INTRODUCTION

An important objective of Deep Sea Drilling Project (DSDP) Leg 65 was to study crustal accretion at an ocean ridge axis with an intermediate-spreading rate for comparison with previously studied sections displaying slow- and fast-spreading rates. The southern Gulf of California was selected for this purpose because the basement displays high seismic velocities (comparable to those observed for Cretaceous basement in the western North Atlantic) and high ambient sedimentation rates, which facilitated penetration of zero-age basement. Four sites were drilled, forming an axial transect immediately south of the Tamayo Fracture Zone (Figs. 1 and 2) and providing a series of characteristic sections into the crust. This chapter attempts to provide a brief synthesis of the results from Leg 65, focusing particularly on the lithology, geochemistry, and paleomagnetic properties of the cored basement material. From these data, we present an interpretation of the processes of magmatic evolution and crustal accretion occurring at the Gulf of California spreading axis.

The Gulf of California represents a young rifted ocean basin in which spreading is believed to have been initiated between three and four m.y. ago. During early Tertiary time, prior to approximately 25 m.y. ago, the entire western margin of North America was marked by a subduction zone along which oceanic lithosphere was being underthrust beneath the continent (Atwater, 1970). Subduction of the Farallon Plate continued until the North American and Pacific plates collided in the vicinity of present-day San Francisco. The San Andreas transform fault then developed, as the triple junction migrated southward from the initial point of plate collision. Approximately 4 to 4.5 m.y. ago, the spreading center jumped inland, causing Baja California to begin rifting away from mainland Mexico.

The present structure and bathymetry of the Gulf of California express this evolving tectonic pattern and in particular reflect a northward transgression from a predominantly dilating to a predominantly transform tectonic regime. The crest of the East Pacific Rise extends northward more or less continuously to the Tamayo Fracture Zone at the mouth of the Gulf. North of the Tamayo Fracture Zone, the Rise is broken into a series of small spreading centers offset by increasingly frequent transform faults oriented obliquely to the axis of the Gulf (Fig. 1). The spreading centers are expressed bathymetrically as deep basins which are partly filled with variable thicknesses of sediment derived from the adjacent land masses. New oceanic crust is currently being formed along the crest of the East Pacific Rise and along the short spreading segments within the Gulf itself. Axial spreading in the Gulf occurs at a rate of about 6 cm/y.

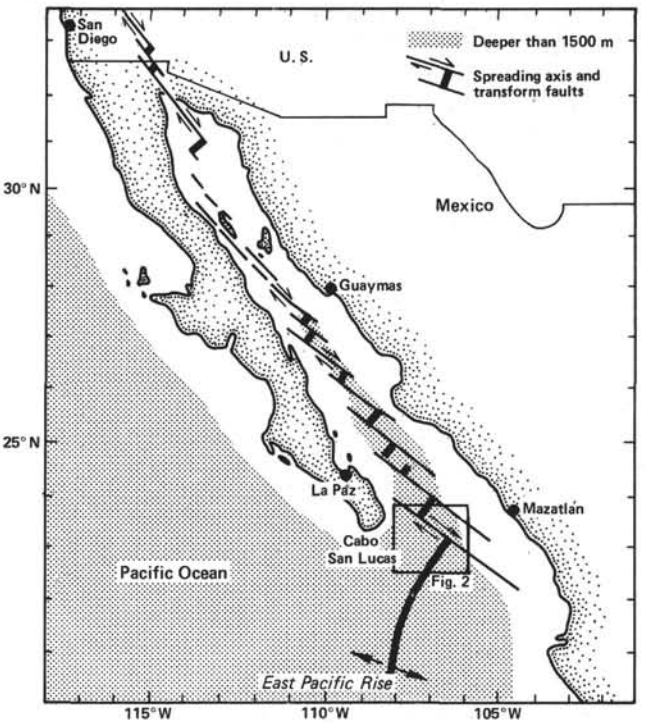

Figure 1. The Gulf of California, showing the Tamayo Fracture Zone and region investigated by drilling at Site 474 (Leg 64) and Sites 482, 483, and 485 (Leg 65).

BASEMENT TOPOGRAPHY

Detailed surveying across the northern end of the East Pacific Rise during the International Phase of Ocean Drilling (IPOD) site surveys revealed a pattern of alternating ridges and flat-floored valleys, symmetrically disposed along opposite sides of the Rise crest (Fig. 3)

[1] Lewis, B. T. R., Robinson, P., et al., *Init. Repts. DSDP*, 65: Washington (U.S. Govt. Printing Office).

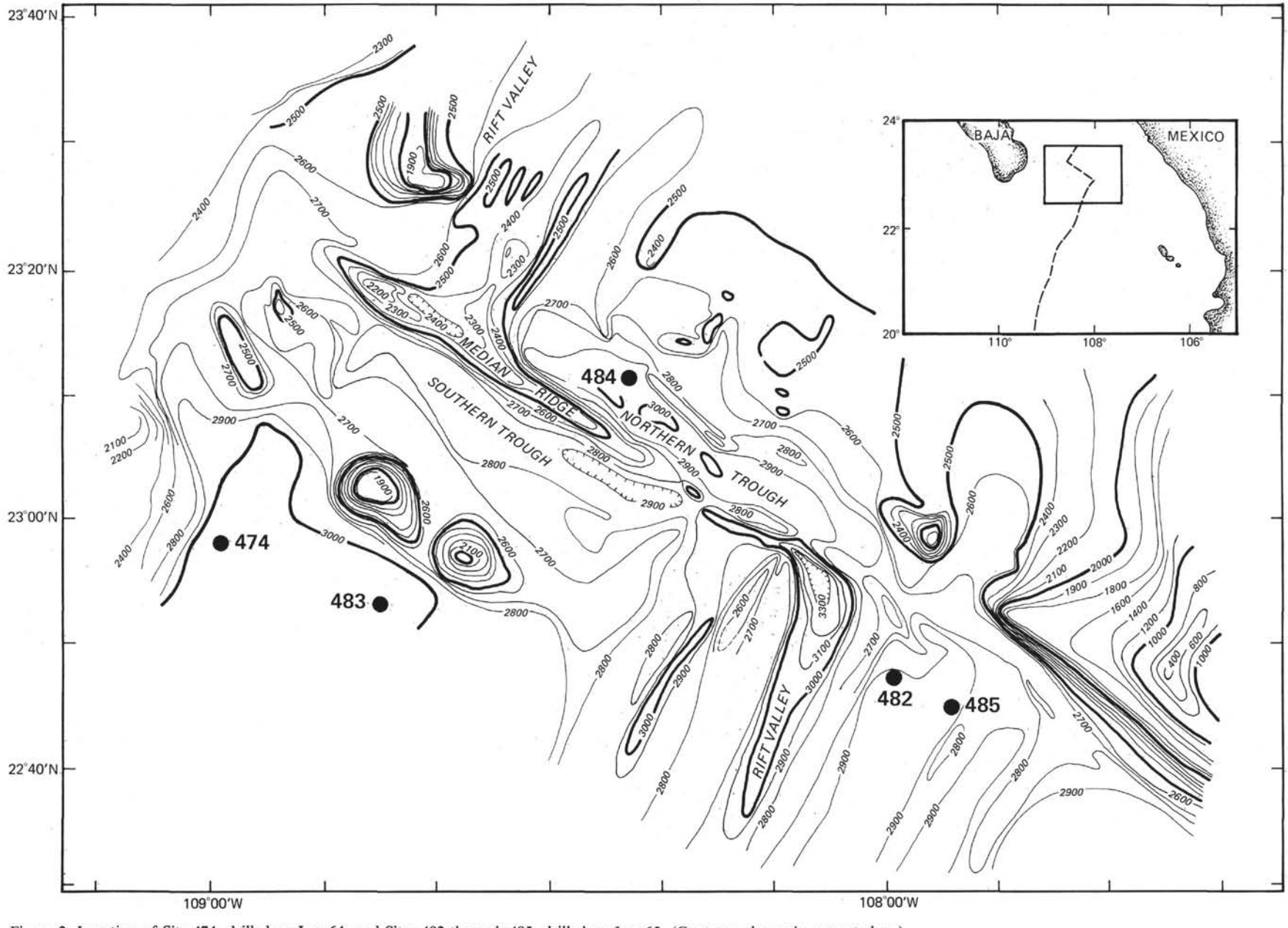

Figure 2. Location of Site 474, drilled on Leg 64, and Sites 482 through 485, drilled on Leg 65. (Contours shown in corrected m.)

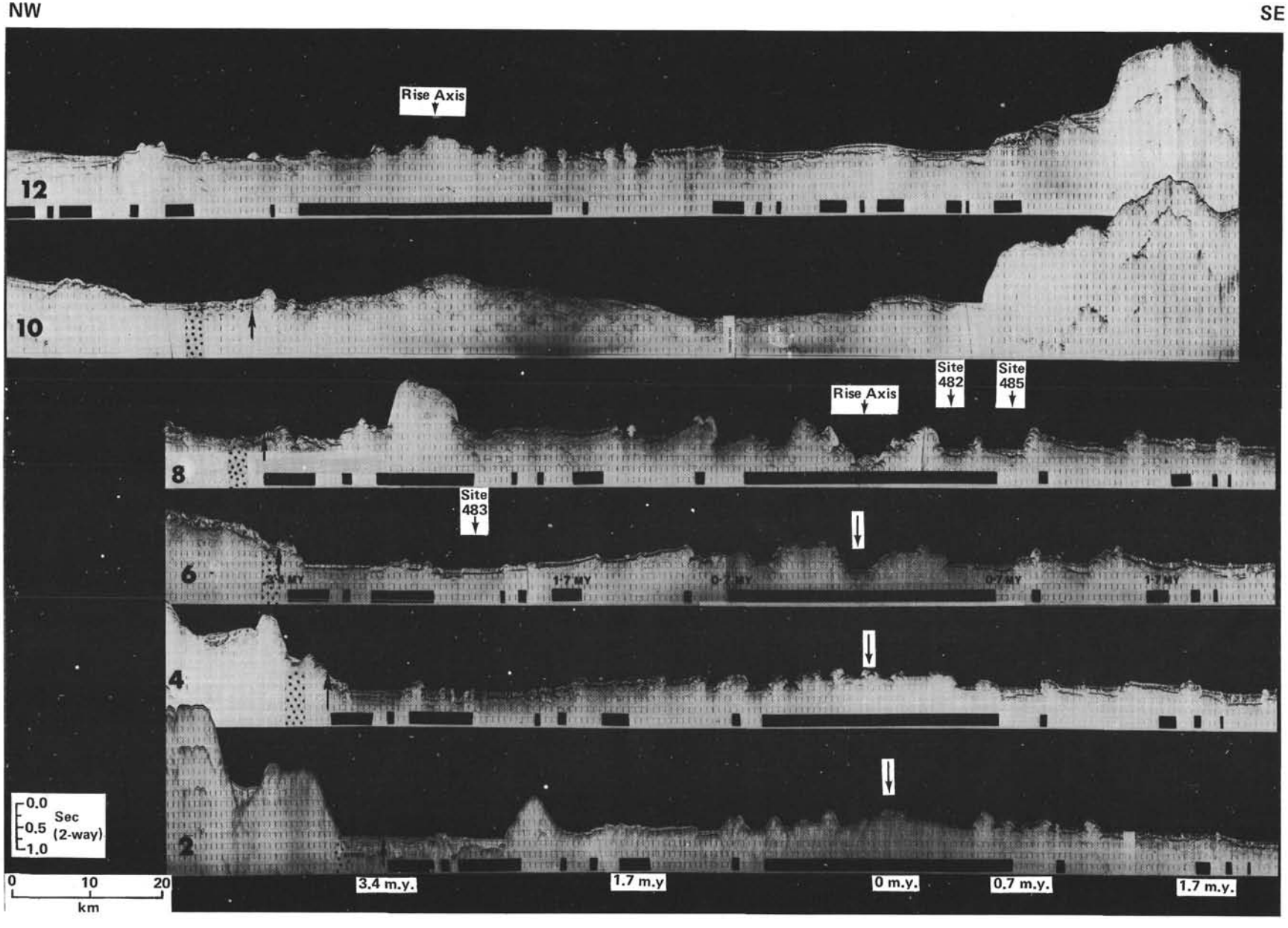

Figure 3. Seismic reflection profiles across the East Pacific Rise in the vicinity of 23°N. Profile 8 lies approximately along the Leg 65 transect. Profiles are arranged sequentially from north (12) to south (2) (after Lewis et al., this volume).

(Lewis et al., this volume). The ridges are discontinuous linear features extending parallel to the rise crest for distances of 5 to 30 km. They range from about 3 to 10 km in width and are asymmetrical in cross section, typically having a relatively steep scarp facing the ridge axis and a more gradual outward-facing slope. The ridges are separated by broad, flat-floored valleys of similar width. The valleys are underlain by variable thicknesses of sediments which show relatively little evidence of tectonic disturbance. The basement/sediment interface is smooth, tilts slightly away from the rise axis, and shows only minor evidence of faulting (Fig. 3).

In the area at the mouth of the Gulf, the axis of the East Pacific Rise exhibits considerable variation in topography. Immediately south of the Tamayo Fracture Zone, the axis is marked by a distinct valley which becomes narrower and shallower to the south and eventually passes into an axial high. The ridge axis immediately north of the Tamayo Fracture Zone is also a topographic high (Fig. 3). Along this segment of the East Pacific Rise, the axial highs are irregular, somewhat rounded features, rather than steep-sided horsts such as those described along the Reykjanes Ridge (e.g., Talwani et al., 1971).

The topography of the axial zone was also observed directly during submersible studies of the Tamayo Fracture Zone and the rift valley to the south (CYAMEX, 1980). This work revealed that within the axial zone, the ridges consist primarily of pillow lavas, whereas the intervening valleys are floored by massive, ponded lava flows with a light, intermittent sediment cover.

DRILLING RESULTS

Basement Lithology

During Leg 65, three principal sites (482, 483, and 485) were drilled on the flanks of the ridge at 23°N, together with a less successful site (484) in the Tamayo Fracture Zone (Fig. 2). These sites, together with one site (474) drilled in older crust on Leg 64 (Curray, Moore, et al., in press), represent an axial transect along an approximate spreading flow line (Fig. 1). Sites 482 and 485 lie east of the ridge axis, whereas Sites 474 and 483 lie to the west. The basement ages for these sites are approximately 0.5 m.y at Site 482, 0.74 m.y. at Site 485, 1.5 to 2.0 m.y. at Site 483, and 4 m.y. at Site 474. All of the sites were located in sediment-filled valleys in order to stabilize the drill string while spudding into basement. Several basement holes were drilled at Sites 482 and 483, but only a single hole penetrated into the basement at each of the other two sites (Fig. 4).

The basement sections at Sites 474 and 483 are similar and consist of an upper sequence of massive basalt units and interlayered sediments underlain by a lower sequence of pillow basalts and thin massive flows (Table 1). The upper basement sequence is about 41 meters thick at Site 474 and about 50 meters thick at Site 483. At Sites 482 and 485, only the upper sequence was penetrated, and this had a minimum thicknesses of approximately 80 and 170 meters, respectively, at the two sites. The sediments interlayered with the upper massive units are lithologically similar to those overlying the acoustic basement and consist largely of hemipelagic material and fine-grained turbidites. The average rates of sediment accumulation above the basement range from a minimum of 7.1 cm/1000 y. at Site 483 to a maximum of 33.4 cm/1000 y. at Site 485, but the rates for individual intervals were often much higher (Benson, this volume). The sedimentation rates during construction of the upper basement sequence are assumed to have been similar.

The massive basalts in the upper basement section range from about 2 to 26 meters in thickness based on drilling rate logs and downhole geophysical logs. The thickest units may comprise several cooling units although internal cooling breaks were rarely recovered. The basalts are aphyric to sparsely phyric, fine to medium grained, and generally display intersertal to subophitic textures. Quenched glassy margins are often preserved at both the upper and lower contacts. Some of the very thick massive basalts in Hole 485A have coarse-grained, glass-free interiors with ophitic textures. Most of the massive units are nonvesicular, but a few (e.g., Unit 7, Hole 483 and Unit 2, Hole 483A) become vesicular toward the margins.

The lower basement sequence penetrated at Sites 483 and 474 consists of pillow and massive basalts with relatively little interlayered sediment. The massive units are similar to those in the upper basement sequence but are usually thinner, ranging from about 2 to 12 meters in thickness. They consist of fine- to medium-grained, aphyric to moderately plagioclase-phyric basalt with intersertal to subophitic textures. Most contain small patches of interstitial glass, partly altered to smectite. Upper glassy margins are often present, but lower selvedges, if they existed, were not recovered. The vesicles are small and sparse, always making up less than 1% of the total volume of the rock. The interlayered pillow basalt sequences are up to about 30 meters thick and show no discernable breaks, although thin sedimentary layers separate pillow from massive units in all cases (Fig. 4). The pillow lavas are characterized by abundant curved glassy margins and by very fine-grained, often quenched, mesostases. The pillow and massive units are mineralogically and chemically distinct (e.g., at Site 483) but appear to be components of related magmatic cycles (Flower et al., this volume).

The pillow basalts are clearly extrusive in origin. Most of the massive units at Sites 482, 483, and 485 are also interpreted as lava flows because of the lack of obvious intrusive contacts, the common presence of glassy mesostases, and the wide lateral extent of individual units. Indurated sediments directly overlying some of the massive units have undergone moderate recrystallization, leading to decreased porosity, the *in-situ* growth of analcite, and the transformation of detrital smectites into saponite and mixed-layer chlorite–smectite (Rangin et al., this volume). Oxygen-isotope data from carbonate material in these zones suggest maximum paleotemperatures of about 65°C. However, the ^{18}O content of

the carbonates could reflect isotope exchange between rock and water rather than baking along the contacts (Rangin et al., this volume).

A likely depositional contact is recorded at the top of Lithologic Unit 7b in Hole 483. The indurated sediment immediately above this contact is clearly imprinted with the vesicular texture of the underlying massive basalt, providing strong evidence for later deposition of the sediment. The base of the succeeding basalt unit, Unit 7a, is also well preserved and consists of a thin (0.5 cm) layer of wrinkled, devitrified glass. The wrinkled contact also implies an eruptive origin for this unit. In contrast, clear evidence for an intrusive origin is observed at Site 474 in the massive units of the upper basement sequence, which is distinctly younger than the underlying pillow sequence (1.8 vs. 3.2 m.y) (Saunders, this volume). At Site 483, a shorter time hiatus is associated with a marked chemical change between the lavas of the upper and lower basement sequences. A few massive units at Site 485 are tentatively interpreted as sills because of their coarse grain size. Units 4 and 5 in Hole 485A are both relatively thick and have groundmass crystals up to 1 cm in length. The sedimentation rates were probably greatest at Site 485 (about 33 cm/1000 y.). For magmatic emplacement in this type of environment, the distinction between flows and sills may be largely semantic: flows that erupted onto unconsolidated sediments may have burrowed laterally into the sediment to produce massive sill-like bodies, chilled above and below against the sediment. Such processes have been documented in the Columbia Plateau, where flows have spread into sedimented lakes (Schmincke, 1967).

Chemical and paleomagnetic studies of the core material have permitted detailed subdivision of the basement into very distinct stratigraphic units. The magma "types" established on shipboard (and refined by Flower et al., this volume) represent compositional groupings which, for the most part, are consistent with groupings based on stable magnetic inclinations (Day, this volume). The average compositions of these magma types are given in Table 2.

Intrasite Stratigraphic Correlation

Multiple holes were drilled at Sites 482 and 483, providing an opportunity to monitor tectonic displacements in the basement. The excellent between-hole correlation established at these sites provides strong evidence for coherent upper basement structure, apparently undisturbed by faulting. At Site 482, individual lithologic units can be correlated petrographically, chemically, and magnetically between three holes (482B, C, and D), located about 1 km apart along a flow line roughly perpendicular to the axis of spreading (Fig. 4A). Eight lithologic units are recognized in Hole 482B, two in Hole 482C, and four in Hole 482D. The uppermost unit in each hole is a massive basalt of Magma Type A (Flower et al., this volume). In Hole 482D Unit 2 also consists of a Magma Type A basalt, but the unit is separated from Unit 1 by a thin sediment layer, whereas in Hole 482C, Unit 2 consists of a Magma Type B basalt. This compositional sequence is the same in both Holes 482B and 482D except that Types A and B are separated by massive units of Type F (Flower et al., this volume).

The correlation of lithologic units and magma types between holes is supported by stable paleomagnetic inclination data (Day, this volume). Lithologic Units 1a (Hole 482B), 1b (Hole 482C), and 2 (482D), all of Magma Type A, have the same stable inclinations to within 1 standard deviation. Unit 1 in Hole 482D, on the basis of a single inclination measurement of 24.0°, is tentatively correlated with Unit 1a of Hole 482C, which has an average inclination of 29.0° ± 1.6°. Lithologic Units 3 (Hole 482D) and 1b (Hole 482B), both of Magma Type F, also have the same average inclinations to within one standard deviation. Units 2 (Hole 482C) and 4 (Hole 482D), both of Magma Type B, also have identical average paleomagnetic inclinations. These two units correlate compositionally and magnetically with Unit 2 in Hole 482B, although the latter displays more variability in inclination. The upper 50 meters of basement at Site 482 thus reflect a marked lithologic, chemical, and magnetic coherence over at least 2 km. This lateral continuity is far greater than that observed at other DSDP sites, especially those in the Atlantic (Hall and Robinson, 1979). The correspondence of stable inclination data to predicted dipole values in the Leg 65 sequences (Day, this volume) is a further indication of the lack of faulting or tectonic rotation during and subsequent to crustal formation. This lateral continuity is also consistent with an extrusive rather than an intrusive origin for most of the massive units.

Similar correlations may be drawn between the holes drilled at Site 483 (Fig. 4B). The upper four units in Holes 483 and 483B, for example, may be correlated on the basis of lithology, chemical composition, and intercalated sedimentary layers. Lithologic Unit 5 in Hole 483, which belongs to Magma Type E, is equivalent to a nonrecovered basalt interval intercalated with sediments in Hole 483B. Likewise, a nonrecovered basalt interval recorded by logging in Hole 483 corresponds to a pillow sequence (Magma Type I) in Hole 483B. At lower levels in the section, several massive units of Magma Type H may be traced between holes. A stratigraphic synthesis of Site 483 thus provides excellent documentation of lateral continuity in the upper levels of the basement formed along this part of the East Pacific Rise.

PROCESSES IN AXIAL MAGMA SYSTEMS

Crustal construction processes at spreading ridges are reflected in the geochemical stratigraphy of the erupted lavas. The observed geochemical patterns and the recognition of upper and lower basement sequences at the Leg 65 sites provide a basis for modeling and interpreting the processes of magmatic evolution which operate at the axial zone of accretion. Most current models of magma generation and evolution at spreading axes relate chemical variation in basalts to variations in crustal spreading rate (e.g., Cann, 1974; Sleep, 1975; Flower, 1980; 1981). Studies of crustal sections formed at the Mid-Atlantic Ridge suggest that accretion at such slow-spreading axes is strongly episodic and is accompanied

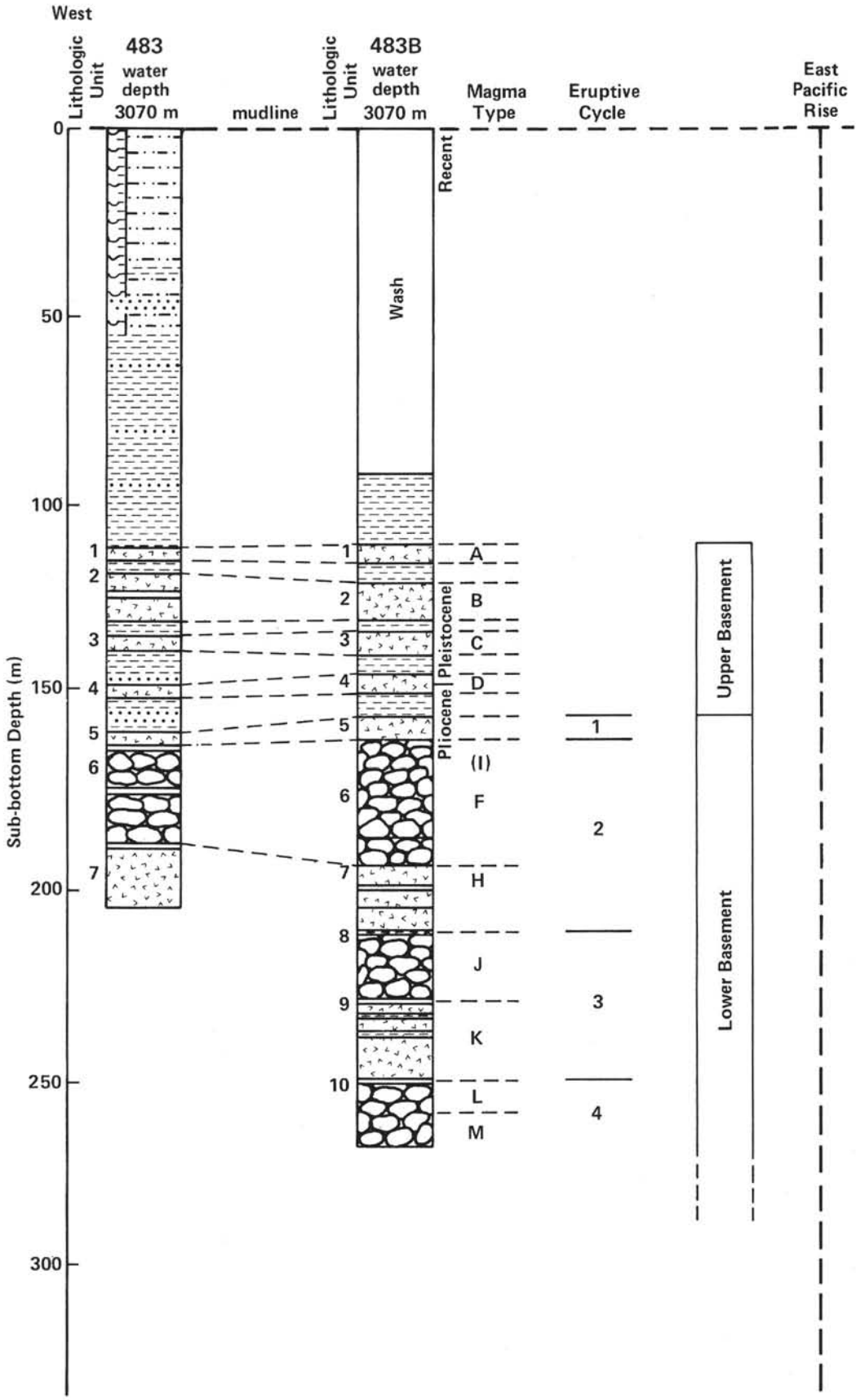

Figure 4. Stratigraphic sections showing correlation of basement lithologic units, magma types, and eruptive cycles at Sites 482, 483, and 485.

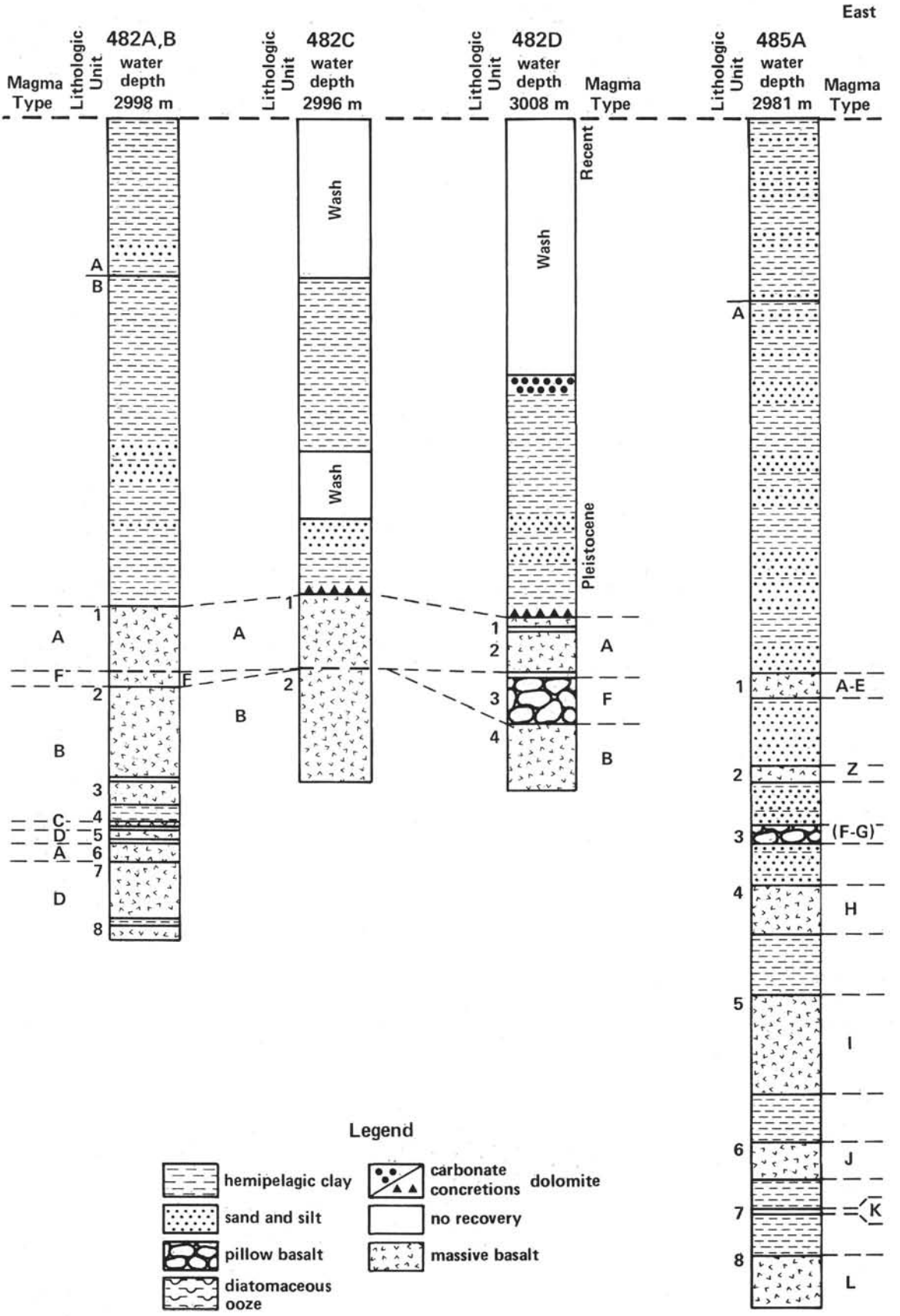

Figure 4. (Continued).

Table 1. Correlation of lithologic units, cooling units, and magma types at Sites 482, 483, and 485.

Hole	Lithologic Unit	Top[a] (m)	Base[a] (m)	Cooling Units	Phenocryst Assemblage	Core-Section (level in cm)	Magma Type[b]
482B	1 Massive basalt	136.5	158.0	1-4	Aphyric	10-7, 8 to 15-1, 115	A, F
	2 Massive basalt	158.0	174.7	10-11	Plagioclase	15-1, 115 to 17-2, 150	A
	Sedimentary intercalation						
	3 Massive basalt	184.1	186.2	12	Plagioclase	18-1, 90 to 18-2, 107	B
	4 Massive basalt	193.5	199.5	13	Plagioclase	19-1, 60 to 20-2, 83	C
	5 Massive basalt	199.5	201.5	14	Plagioclase-Clinopyroxene	20-2, 83 to 20-3, 130	D
	6 Massive basalt	201.5	205.0	15	Plagioclase-Clinopyroxene-Olivine	20-3, 130 to 21-3, 50	E
	7 Massive basalt	205.0	220.3	16	Plagioclase-Clinopyroxene-Olivine	21-3, 50 to 23-1, 30	D
	Sedimentary intercalation						
	8 Massive basalt	224.7	229.0	17	Aphyric	24-1, 25 to 24-3, 130	D
482C	1 Massive basalt	135.5	157.0	1-2	Aphyric	9-1, 60 to 12-1, 0	A
	2 Massive basalt	157.0	184.0	3-7	Plagioclase-Clinopyroxene-Olivine	12-1, 0 to 15-4, 145	F, B
482D	1 Massive basalt	138.0	139.6	1-2	Aphyric	8-1, 0 to 8-2, 30	A
	Sedimentary intercalation						
	2 Massive basalt	141.7	154.0	3	Aphyric	9-1, 15 to 10-3, 60	F, E
	Sedimentary intercalation						
	3 Pillow basalt?	154.1	169.6	4-10	Aphyric	10-3, 65 to 12-1, 130	F
	4 Pillow basalt?	169.6	186.5	11-16	Plagioclase	12-1, 130 to 13-3, 35	B
483	1 Massive basalt	110.0	111.0	1	Plagioclase-Olivine	13-4, 5 to 13-4, 95	A
	Sedimentary intercalation						
	2 Massive basalt	115.0	127.0	2a, b	Aphyric	14-1, 5 to 15-2, 128	B
	Sedimentary intercalation						
	3 Massive basalt	127.0	135.8	3	Aphyric	15-2, 128 to 16-3, 12	C
	Sedimentary intercalation						
	4 Massive basalt	142.2	145.0	4	Aphyric	17-1, 18 to 17-3, 24	D
	Sedimentary intercalation						
	5 Massive basalt	156.5	160.1	5	Aphyric	18-4, 130 to 19-1, 10	E
	Sedimentary intercalation						
	6a Pillow basalt?					unrecovered	F?
	Sedimentary intercalation						
	6b Pillow basalt?	169.0	186.5	6-27	Plagioclase-Clinopyroxene-Olivine	20-1, 5 to 22-4, 60	F
	6c Massive basalt	186.5	188.5	28	Plagioclase-Olivine	22-4, 60 to 23-2, 20	F-Plagioclase
	6d Pillow basalt?	188.5	190.0	29-30	Plagioclase-Clinopyroxene-Olivine	23-2, 20 to 23-2, 150	F
	Sedimentary intercalation						
	7a Massive basalt	191.5	200.3	31-34	Plagioclase-Olivine	24-1, 5 to 26-1, 40	H
	Sedimentary intercalation						
	7b Massive basalt	200.4	204.5	35	Plagioclase	26-1, 50 to 26-3, 150	H
483B	1 Massive basalt	110.0	111.3	1	Plagioclase-Olivine	2-7, 0 to 3-1, 75	A
	Sedimentary intercalation						
	2 Massive basalt	111.3	127.0	2	Aphyric	3-1, 75 to 4-7, 20	B
	Sedimentary intercalation						
	3 Massive basalt	133.0	136.4	3	Aphyric	7-1, 7 to 7-3, 75	C
	Sedimentary intercalation						
	4 Massive basalt	137.6	146.8	4	Aphyric	8-1, 10 to 9-1, 44	D
	Sedimentary intercalation						
	5a Pillow basalt	169.0	175.0	6-10	Plagioclase-Olivine-Clinopyroxene	12-1, 0 to 13-1, 10	I
	5b Pillow basalt	175.0	184.6	11-22	Plagioclase-Olivine-Clinopyroxene	13-1, 10 to 15-1, 6	F
	Sedimentary intercalation						
	6a Massive basalt	194.0	197.3	23	Aphyric	17-1, 0 to 17-3, 45	H
	Sedimentary intercalation						
	6b Massive basalt	199.0	204.6	24	Aphyric	18-1, 0 to 19-1, 65	H
	Sedimentary intercalation						
	6c Massive basalt	204.6	206.2	25	Aphyric	19-1, 65 to 19-2, 85	H
	6d Massive basalt	206.2	210.5	26	Plagioclase-Olivine-Clinopyroxene	19-2, 85 to 20-2, 65	H
	Sedimentary intercalation						
	7a Pillow basalt	211.1	213.0	27	Plagioclase-Olivine	20-2, 130 to 20-3, 30	H?
	7b Pillow basalt	213.0	227.7	28-56	Plagioclase-Clinopyroxene-Olivine	21-1, 0 to 24-1, 145	J
	Sedimentary intercalation						
	8a Massive basalt	227.7	232.4	57	Plagioclase-Clinopyroxene-Olivine	24-1, 145 to 25-2, 5	K
	Sedimentary intercalation						
	8b Massive basalt	232.6	236.9	58	Plagioclase-Olivine	25-2, 20 to 26-1, 150	K
	Sedimentary intercalation						
	8c Massive basalt	237.0	249.5	59	Plagioclase-Olivine	26-2, 5 to 29-1, 65	K
	Sedimentary intercalation						
	9 Pillow basalt	249.5	267.0	60-82	Plagioclase-Olivine-Clinopyroxene	29-1, 65 to 32-3, 82	L, M
483C	1 Massive basalt	109.5	114.0	1	Aphyric	4-2, 47 to 4-5, 120	A
485A	1 Massive basalt	153.5	159.4	1-5	Plagioclase-Olivine-Clinopyroxene	11-3, 55 to 13-1, 140	A-E
	Sedimentary intercalation						
	2 Massive basalt	180.5	184.0	?	Plagioclase	17-1, 0 to 18-1, 58	Z
	Sedimentary intercalation						
	3 Pillow basalt	201.5	202.0	?	Plagioclase	22-1, 0 to 22-1, 3	?
	Sedimentary intercalation						
	4 Massive basalt	212.0	226.2	8	Plagioclase-Olivine	23-1, 50 to 26-1, 20	H
	Sedimentary intercalation						
	5 Massive basalt	239.5	270.4	9	Plagioclase	29-1, 0 to 33-2, 95	I
	Sedimentary intercalation						
	6 Massive basalt	277.5	294.0	10	Plagioclase-Olivine	34-1, 56 to 35-6, 55	J
	Sedimentary intercalation						
	7 Massive basalt	293.6	298.7	11	Plagioclase	36-3, 64 to 36-cc, 31	K
	Sedimentary intercalation						
	8 Massive basalt	314.5	328.5	12	Plagioclase	38-2, 2 to 39-5, 60	L

[a] Calculated from core log and corrected for spacers.
[b] See Table 2.

Table 2. Average magma type compositions[a] at Sites 482, 483, and 485 (after Flower et al., this volume).

Magma Type	SiO_2	TiO_2	Al_2O_3	FeO*	MnO	MgO	CaO	Na_2O	K_2O	P_2O_5
Site 482										
A	50.58	1.82	14.71	10.25	0.21	7.96	11.63	2.58	0.09	0.16
B	50.85	1.35	14.94	9.94	0.18	8.20	11.93	2.46	0.04	0.11
C	51.20	1.28	14.70	10.03	0.17	8.16	12.00	2.30	0.06	0.11
D	50.35	1.56	15.54	9.88	0.18	7.42	12.25	2.65	0.04	0.14
E	50.67	1.89	14.67	10.32	0.18	7.85	11.54	2.67	0.06	0.17
F	50.47	1.44	15.14	10.12	0.18	8.04	11.95	2.48	0.06	0.12
G	50.79	2.15	14.40	11.40	0.19	6.87	11.02	2.86	0.11	0.20
H	50.55	1.43	14.96	10.05	0.18	8.31	11.90	2.46	0.05	0.11
Site 483										
B	51.04	1.24	15.25	9.17	0.16	8.04	12.31	2.64	0.06	0.09
C	50.78	1.39	14.77	9.97	0.17	7.86	12.17	2.73	0.06	0.10
D	49.84	1.01	16.87	8.27	0.16	9.09	12.38	2.27	0.04	0.07
E	51.09	1.85	16.47	8.48	0.15	7.44	10.99	3.19	0.16	0.18
F	50.34	1.86	15.08	10.72	0.20	7.14	11.80	2.61	0.09	0.17
H	50.33	2.18	14.54	11.41	0.19	7.28	10.97	2.80	0.10	0.21
I	50.06	1.58	15.70	10.36	0.20	7.22	12.07	2.62	0.06	0.13
J	50.40	1.73	15.04	10.25	0.21	7.56	11.93	2.65	0.08	0.15
K	50.36	1.82	14.67	10.71	0.19	7.67	11.63	2.72	0.09	0.16
L	50.42	1.81	14.91	10.52	0.23	7.60	11.60	2.65	0.11	0.16
M	50.42	1.62	15.59	9.63	0.20	7.64	11.94	2.68	0.12	0.15
Z	50.87	1.33	14.71	9.99	0.17	7.75	12.37	2.65	0.05	0.10
Site 485										
A	50.00	1.54	17.36	9.37	0.13	7.13	11.25	3.08	0.03	0.10
B	50.50	2.09	13.93	11.93	0.23	6.83	11.62	2.60	0.09	0.19
C	50.62	2.12	13.83	12.11	0.23	6.89	11.38	2.56	0.07	0.19
E	50.83	2.04	14.18	11.72	0.21	7.12	11.11	2.54	0.06	0.19
H	50.26	2.24	14.83	11.40	0.17	7.07	10.76	2.93	0.14	0.20
I	50.10	2.05	14.71	11.07	0.19	7.82	11.12	2.62	0.13	0.18
J	50.63	1.79	14.59	10.68	0.18	7.78	11.48	2.60	0.06	0.15
K	49.95	2.48	19.61	9.85	0.19	6.41	7.55	3.68	0.06	0.21
L	50.44	1.87	15.00	10.74	0.19	7.68	11.27	2.58	0.06	0.16
Z	49.97	2.33	15.47	12.09	0.19	7.85	8.87	2.98	0.05	0.20

Note: FeO* = total iron as FeO.
[a] Values given in wt.%; normalized and corrected for carbonate.

by extensive tectonic disruption of the crust (Hall and Robinson, 1979; Flower and Robinson, 1979; 1981b). The resulting crustal segments are composed of overlapping lenses with little lateral continuity. Compositional variations in these lenses reflect repetitive magmatic cycles, usually passing from most evolved at the base to most primitive at the top (Flower and Robinson, 1981b). In many cases, the magmas appear to have undergone extensive crystal fractionation in separate subrift magma chambers.

Flower (1980; 1981) has observed that basalts formed at slow-spreading axes may be characterized by the massive accumulation of calcic plagioclase and by widespread phenocryst reaction morphologies suggestive of polybaric fractionation regimes, while those generated along fast-spreading axes appear to have formed in low pressure (isobaric) systems. Kinematic and thermal models (e.g., Sleep, 1975; 1978) also imply changes related to spreading rate, specifically, a tendency toward isobaric, open-system fractionation along fast-spreading axes and polybaric, closed-system fractionation along slow-spreading axes (Flower 1980; 1981; Nisbet and Fowler, 1978). The physical and chemical effects of these differences on eruptive magma chemistry have been discussed by Sparks et al. (1980), Stolper and Walker (1980), O'Hara (1977), and O'Hara and Mathews (1981), and provide a perspective from which to view the results from the Gulf of California.

The compositional variation of the Leg 65 basalts is intermediate in type between that observed along fast-spreading segments of the East Pacific Rise and Nazca Plate and the slow-spreading Mid-Atlantic Ridge (Fig. 5). Oxide and trace element studies and least-squares mass balance models strongly suggest that some of the massive and pillow units recovered (e.g., Magma Types 482-D; 483-D, -F, -H, and -K; 485-A, -E, -H, and -I) display evidence of incipient, and in a few cases, substantial plagioclase accumulation (Flower et al., this volume). This accumulation is evident mainly from compositional variations within magma types and appears to be superimposed on a generalized "cotectic" liquid fractionation trend represented by variations in glass composition (Flower and O'Hearn, this volume) and by typical "fast-spreading" whole-rock variation patterns (e.g., Clague and Bunch, 1976). The more extensive plagioclase accumulation in basalts formed at slow-spreading axes tends to obscure liquid-type trends, whereas the intermediate character of the Gulf of California variation pattern allows both effects to be discerned.

It is reasonable to interpret geochemical variations in the Leg 65 basalts in terms of separate fractionation episodes involving simple phenocryst redistribution in more-or-less cogenetic parent magmas (Flower et al., this volume). However, close scrutiny of the petrographic and chemical characteristics of the Leg 65 basalts leads to some important constraints on the extent to which open- vs. closed-system fractionation may operate in this environment. In comparatively rare phyric lavas, the phenocrysts of clinopyroxene and plagioclase are frequently resorbed, and the plagioclase shows oscillatory zoning. Moreover, basalts with chemical compositions reflecting the most extensive accumulation of plagioclase are aphyric or, at most, very sparsely phyric. Flower et al. (this volume) interpret these lavas as "cryptocumulates," resulting from accumulation of plagioclase during temporary stagnation of the magma supply, followed by resorption of plagioclase during reheating as a consequence of mixing with newly injected primitive magma. This hypothesis is supported by two lines of evidence: (1) the least phyric "cryptocumulates" are the most MgO-rich (e.g., Magma Types 483-D; 485-A), and (2) the major and trace element variation within these magma types (Fig. 5) is strongly suggestive of mixing (as opposed to fractional crystallization).

In summary, it is tentatively concluded that fractionation of magma ascending beneath this portion of the axis of the East Pacific Rise occurs neither in a single continuously evolving, steady-state magma chamber nor in a simple, linear sequence of discrete, closed systems. We infer that construction of any given vertical section of the crust involves the operation of several separate systems, each of which may represent a steady-state system during its own finite existence. Although it is difficult to "invert" geochemical parameters in the erupted products of such systems to define cyclic evolution (O'Hara and Mathews, 1981), real constraints can be derived from stratigraphic, and hence chronologic, relationships among the different eruptive units. For example, the chemical stratigraphy at Site 483, based on variations in Zr-Ti, Zr-Y, and Ti-Y element pairs with $Mg/Mg + Fe^{2+}$, reflect a distinct cyclic pattern defined by successive chemical types or groups of types. Four cy-

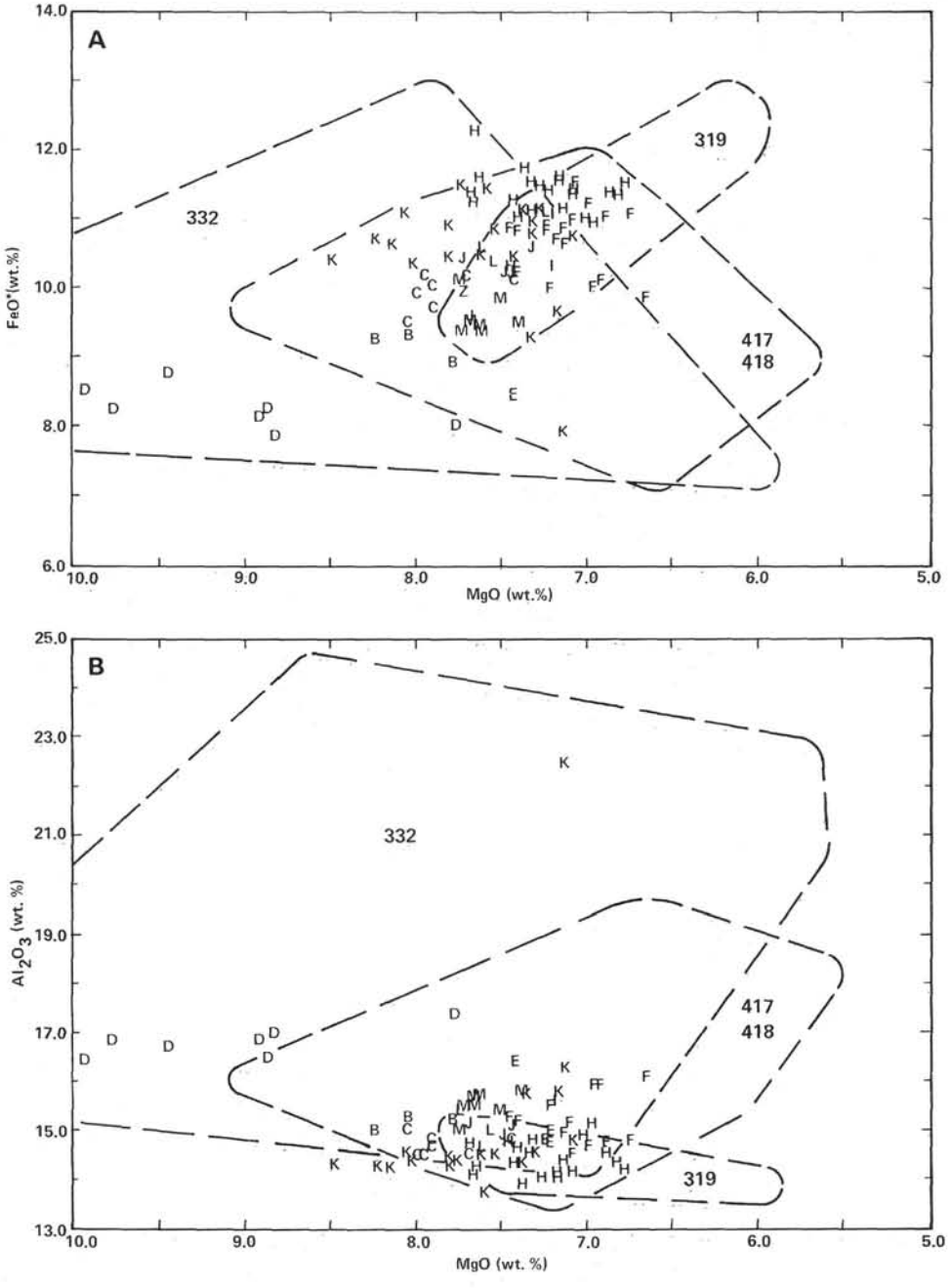

Figure 5. Oxide variation at Site 483 compared with variations in crust formed at a slow-spreading ridge (Sites 332, 417, and 418 on the Mid-Atlantic Ridge) and a fast-spreading ridge (Site 319 on the Nazca Plate). A. FeO* vs. MgO; B. Al_2O_3 vs. MgO. (Letters represent magma types at Site 483. Data from Flower et al. [this volume; 1977] and Rhodes et al. [1976].

cles are recognized consisting of Chemical Types E, I-F-H, J-K, and L-M (Flower et al., this volume). Each cycle comprises a series of massive units succeeded by pillow basalts. The small but consistent differences in low-K_D element abundances between cyclic associations (Fig. 6) may be attributed to one or more of the following: (1) a heterogeneous mantle source, tapped variably in time and space; (2) changes in the percent of partial melting for successive batches of mantle-derived magmas; and (3) differences in the longevity of steady-state (periodically refilled and depleted) magma systems (O'Hara and Mathew, 1981) and thus, in the duration of cyclic fractionation.

At Sites 474, 483, and, to a lesser extent, 485, a distinct compositional change marks the transition from the lower to upper basement sequences (Figs. 5 and 6). At Site 474, this transition corresponds to a significant time hiatus (Saunders, this volume) and at Site 483, it corresponds to a paleomagnetic polarity reversal (Day, this volume). The first basalt unit in the upper basement section at Site 483 (Magma Type 483-D) displays unambiguous evidence of plagioclase accumulation, magma

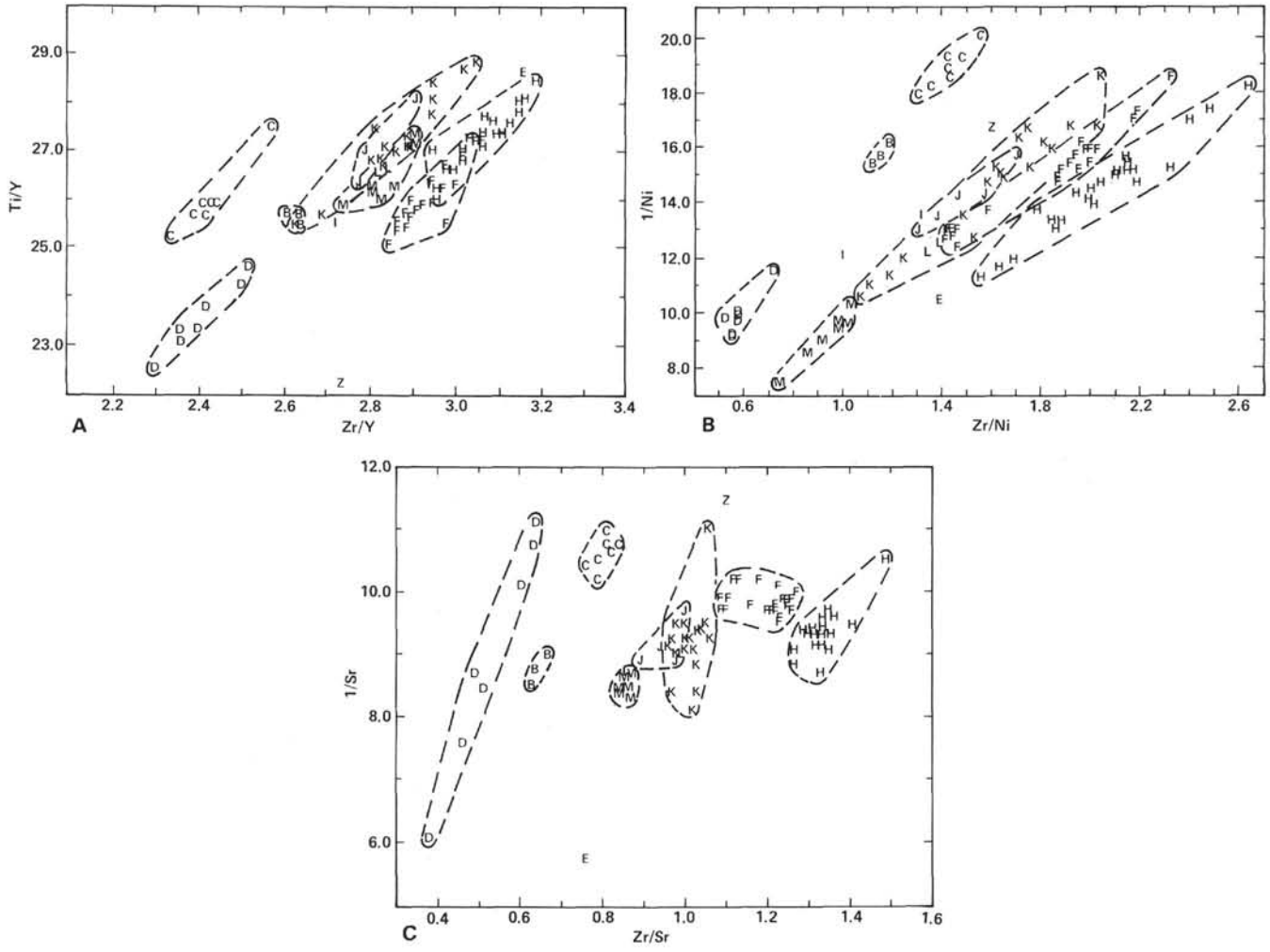

Figure 6. Trace element variation at Site 483 according to magma type. A. Ti/Y vs. Zr/Y; B. 1/Ni vs. Zr/Ni; C. 1/Sr vs. Zr/Sr. (Deflection of variation from straight-line trends is attributable in A to source-related processes (such as variable partial melting or mantle heterogeneity) and/or to fractionation in a steady-state "open" system. The deflections in B result from mafic phase fractionation. Those in C result from plagioclase fractionation or accumulation. Straight-line variation for all parameters is consistent with binary mixing [cf. Langmuir et al., 1978].) (Data from Flower et al., this volume.)

mixing and reheating, and possibly the inception of a new cyclic phase. At Site 474, the upper massive units may represent later off-axis volcanism (Saunders, this volume), perhaps related to a renewed phase of rifting. At the Leg 65 sites, we interpret the upper basement units as widespread flows that originated at the spreading axis.

CRUSTAL ACCRETION PROCESSES

Slow-spreading ridges such as the Mid-Atlantic Ridge are usually characterized by distinct and continuous axial rift valleys. Two models have been proposed to explain the continued existence of such rift valleys during crustal accretion, the "suction" model of Lachenbruch (1976) and the "necking" model of Tapponier and Francheteau (1978). Both models assume that the morphology of the ridge axis is a steady-state phenomenon and that it reflects a passive response to the rifting of rigid plates.

It is clear from ridge transect profiles that the axial valley on the East Pacific Rise at 23°N is not a continuous feature since it passes into an axial high both to the north and south. If the spreading rate is assumed to be constant, the morphologic variations along the ridge axis must reflect either differences in the rate of magma supply or tectonic disturbance. The axial highs on this segment of the East Pacific Rise differ markedly in morphology from the horst-like features found on the Reykjanes Ridge (Talwani et al., 1971), and there is no evidence that they have formed by faulting or uplift in the axial valley.

If the axial valley at the Rise crest were a steady-state feature, the upper crust should everywhere consist of interlayered massive basalts and sediments similar to the sections drilled on Leg 65, and the linear ridges on the flanks of the Rise would simply mark upfaulted crustal segments. Although the ridges have not been sampled by drilling, several lines of evidence strongly suggest that they are underlain by crust of a different character from that drilled in the sediment-filled valleys: (1) The ridges are irregular, asymmetric, somewhat rounded features, whereas the upper basement surface beneath the

valleys is always smooth and regular (Fig. 3); (2) Dredging on the flanks of the ridges has recovered glass-rich pillow lavas without the interlayered sediments found by drilling in the valleys; (3) The interlayered massive basalts and sediments drilled on Leg 65 presumably accumulated in topographic lows, probably by ponding in the axial valley. Since ponding cannot take place where the Rise axis is marked by a topographic high and dredging indicates that the axial highs are composed largely of pillow piles, the crustal section must vary along the Rise axis; (4) If the axial valley south of the Tamayo Fracture Zone is a steady-state feature, as proposed for the Mid-Atlantic Ridge axis, and all crustal accretion occurs within the valley, constructional topographic features should disappear once the crust has migrated out of the axial valley and a uniform layer of sediment would be expected to form above the basement. Instead, the Rise flanks at 23°N are marked by a highly symmetrical pattern of alternating basalt ridges and sedimented valleys (Lewis, 1979).

From these considerations and the geochemical evidence discussed above, we conclude that crustal accretion along this segment of the East Pacific Rise can best be explained in terms of episodic processes involving variable rates of magma supply, both from the upper mantle to the magma reservoir systems and from the latter to the surface of the ocean floor. At present, the longitudinal distance between axial highs and lows is estimated to be about 90 km (Lewis, 1979). If these features reflect a propagating magma source (Lewis, 1979), they suggest a longitudinal migration rate for eruptive activity of about 50 cm/y., which corresponds to an average periodicity of 0.35 m.y.

Our model for the evolution of this ridge segment is summarized in Figure 7. During periods of low magma supply, continued spreading produces an axial valley such as that observed in the Leg 65 transect (Fig. 7A). In some cases, this rifting may be accompanied by normal faulting and uplift of the ridge flanks. Where this occurs the upper basement surface in the adjacent valleys may be tilted somewhat away from the rift axis. In other cases, where there is no evidence of tilting, the rifting probably occurred without significant uplift and faulting. The resulting crustal sections formed during periods of low magma supply consist of pillow lavas and thin massive flows, corresponding to the lower basement sequences penetrated at Sites 474 and 483. Sediments accumulate rapidly in the axial rift, in part by turbidity current deposition. Continued spreading initiates a new rifting episode within the axial valley, perhaps related to a longitudinally propagating magma source, allowing a series of relatively rapid eruptions to build an axial ridge (Fig. 7B). During construction of these axial ridges, the eruptions are episodic on a fine scale with variable amounts of magma being emplaced during each episode. Relatively voluminous eruptions produce massive flows that pond in the axial low to either side and spread across the sediment-covered surface (Fig. 7C). In the waning stages of the more voluminous pulses and during less voluminous eruptions, pillow basalts accumulate in quenched mounds close to the eruptive source. Finally, as the magma supply to the axial zone again diminishes, a new rift forms, starting the cycle anew (Figure 7D).

In this model, the massive units in the upper basement sequences at the Leg 65 sites are related to the same eruptive episodes that produced the linear axial ridges. This interpretation is supported by the evidence for a time hiatus and a marked geochemical transition at the boundary between the upper and lower basement sequences. Additional evidence for small scale periodicity resulting in relatively voluminous massive flows and small mounds of pillows comes from the following: observations of the axial topography using submersibles (e.g., CYAMEX, 1981), from the chemically defined eruption/fractionation cycles (massive flows followed by pillow sequences) drilled on Leg 65, and from paleomagnetic and sedimentary indications of episodic crustal construction.

An episodic magma supply is also interpreted from basement stratigraphy in the Atlantic Ocean (e.g., Flower et al., 1977; Byerly and Wright, 1978; Flower and Robinson, 1979) and from comparative studies of the FAMOUS and AMAR segments of the Mid-Atlantic Ridge (Bryan and Moore, 1977; Ballard et al., 1978). Comparisons of chemical and lithologic stratigraphy and longitudinal variations in morphology between intermediate-spreading rate segments of the East Pacific Rise and the slow-spreading Mid-Atlantic Ridge lead to two contrasting dynamic models. At the faster-spreading axis, accretionary processes reflect both large and small scale variations in magma supply. The morphology of the ridge axis varies longitudinally, probably in response to a propagating magma source. Accreted crustal segments are laterally continuous and tectonically undisturbed. At the slow-spreading axis, small scale fluctuations in magma supply are also characteristic, but the absence of large scale variations allows perpetuation of an axial rift. Crustal accretion takes place by subsidence and the periodic burial of eruptive lenses under new lava. These contrasting tectonic patterns are evident primarily from the distinctive longitudinal character of East Pacific Rise vs. Mid-Atlantic Ridge topography and the evidence for iterative tectonic rotation in slow-spreading, as opposed to faster-spreading crust (Hall and Robinson, 1979; Flower and Robinson, 1979; 1981a; 1981b). This model is further supported by the well-known relationship between ridge topography and spreading rate (e.g., Cann, 1974) whereby fast-spreading axes are invariably characterized by their lack of rifts in contrast to slow-spreading axes.

To summarize, the geometric and temporal character of magma supply and fractionation systems in the 23°N segment of the East Pacific Rise are intermediate in character between those predicted for fast-spreading sections of East Pacific Rise and the slow-spreading Mid-Atlantic Ridge axis. The Gulf of California magma systems resemble those of the Mid-Atlantic Ridge in being transient, possibly polybaric, and in giving rise to plagioclase-cumulate magmas. In contrast, the emplacement of magma appears to take place under relatively stable tectonic conditions, probably more typical of faster-spreading environments in which tectonic adjustments to episodic spreading are relatively infrequent.

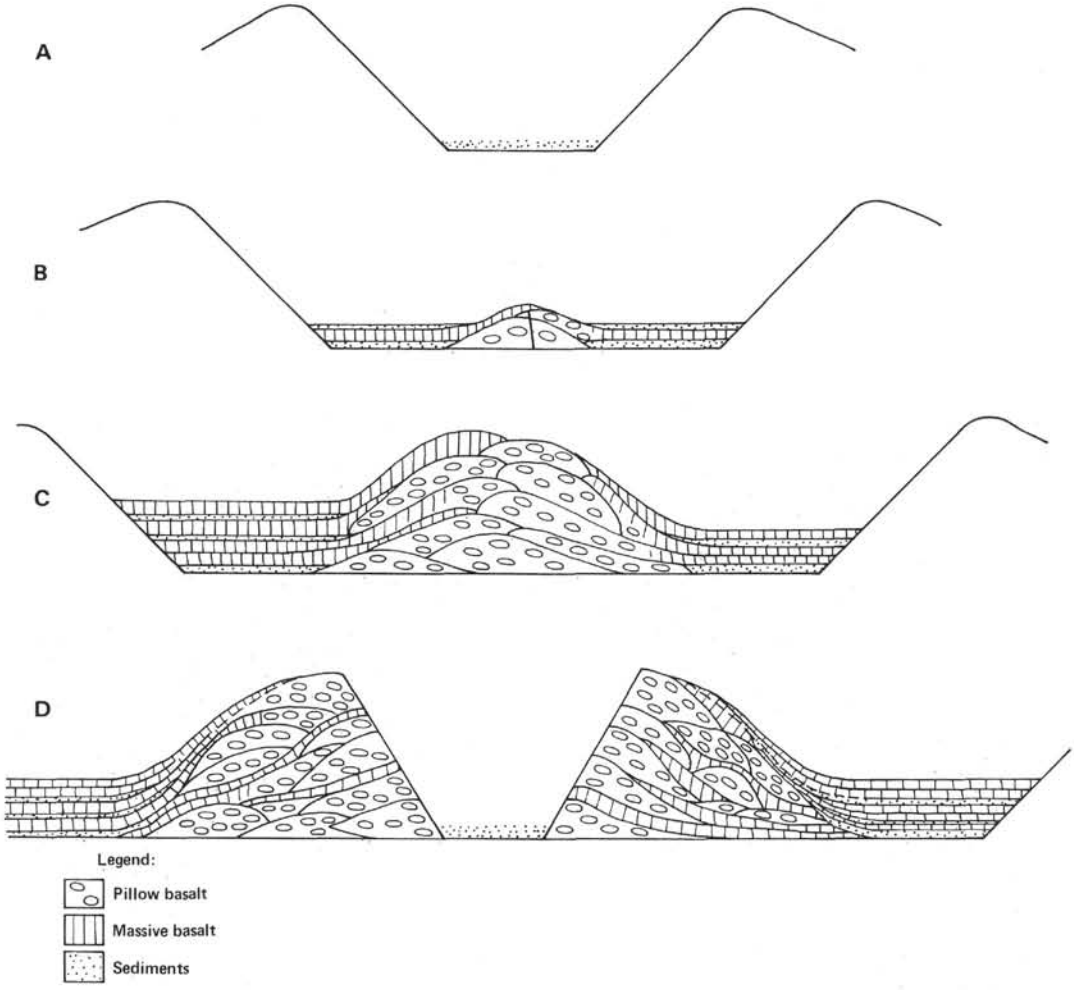

Figure 7. Schematic diagram illustrating model for crustal accretion along the East Pacific Rise axis at 23°N. A. Rifting during period of relatively low magma supply produces axial valley. B. Sedimentation in axial valley is accompanied by renewed volcanism along rift axis. C. Rapid magma production and emplacement builds axial high composed largely of pillow lavas. Massive flows and sills are emplaced on flanks of axial high, forming upper basement section composed of interlayered sediments and massive basalts. D. Renewed rifting during period of low magma supply forms new axial valley, starting the cycle again.

ACKNOWLEDGMENTS

We thank the captain and crew of the D/V *Glomar Challenger* for their efforts in making Leg 65 a success. Claude Rangin provided many lucid descriptions of features observed during submersible studies of the Rise crest, and James Mehegan assisted with the drafting of several of the figures.

REFERENCES

Atwater, T., 1970. Implications of plate tectonics for the Cenozoic tectonic evolution of western North America. *Geol. Soc. Am. Bull.*, 81:3513–3536.

Ballard, R. D., Atwater, T., Stakes, D., et al., 1978. AMAR 78 preliminary results IV. AMAR rift valley—Evidence for cycles in the evolution of rift valleys. *Trans. Am. Geophys. Union, Eos*, 59: 1198–1199.

Byerly, G., and Wright, T. L., 1978. Origin of major-element chemical trends in DSDP Leg 37 basalts, Mid-Atlantic Ridge. *J. Volcanol. Geotherm. Res.*, 3:229–279.

Bryan, W. B., and Moore, J. G., 1977. Compositional variation of young basalts in the Mid-Atlantic Ridge rift valley near 36°50′N. *Geol. Soc. Am. Bull.*, 88:556–570.

Cann, J., 1974. A model for oceanic crustal structure developed. *Geophys. J. R. Astron. Soc.*, 39:169–187.

Clague, D. A., and Bunch, T. E., 1976. Formation of ferrobasalt at East Pacific midocean spreading centers. *J. Geophys. Res.*, 81: 4247–4256.

Curray, J. R., Moore, D. G., et al., in press. *Init. Repts. DSDP*, 64: Washington (U.S. Govt. Printing Office).

CYAMEX Scientific Group, 1981. First manned submersible dives on the East Pacific Rise, 21 N. (Project RITA): General results. *Mar. Geophys. Res.*, 4:365–379.

Flower, M. F. J., 1980. Accumulation of calcic plagioclase in ocean-ridge tholeiite: An indication of spreading rate? *Nature*, 287: 530–532.

_____, 1981. A thermal-kinematic model for ocean-ridge magma fractionation. *J. Geol. Soc. Lond.*, 138:695–712.

Flower, M. F. J., and Robinson, P. T., 1979. Evolution of the 'FAMOUS' ocean ridge segment: Evidence from submarine and deep drilling investigations. *In* Talwani, M., et al., (Eds.), *Deep Drilling Results in the Atlantic Ocean: Ocean Crust* (Vol. 2): Washington (American Geophysical Union), Maurice Ewing Ser., pp. 314–330.

_____, 1981a. Basement drilling in the western Atlantic Ocean 1. Magma fractionation and its relation to eruptive chronology. *J. Geophys. Res.*, 86:6273–6298.

_____, 1981b. Basement drilling in the western Atlantic Ocean 2. A synthesis of construction processes at the Cretaceous ridge axis. *J. Geophys. Res.*, 86:6299–6309.

Flower, M. F. J., Robinson, P. T., Schmincke, H.-U., and Ohnmacht, W, 1977. Magma fractionation systems beneath the Mid-Atlantic Ridge at 36–37°N. *Contrib. Mineral. Petrol.*, 64:167–195.

Hall, J. M., and Robinson, P. T., 1979. Deep crustal drilling in the North Atlantic Ocean. *Science*, 204:573–586.

Lachenbruch, A. H., 1976. Dynamics of a passive spreading center. *J. Geophys. Res.*, 81:1883–1902.

Langmuir, C. H., Bender, J. F., Bence, A. E., et al., 1977. Petrogenesis of basalts from the FAMOUS area, Mid-Atlantic Ridge. *Earth Planet. Sci. Lett.*, 36:133–156.

Lewis, B. T. R., 1979. Periodicities in volcanism and longitudinal magma flow on the East Pacific Rise at 23°N. *Geophys. Res. Lett.*, 6:753–756.

Nisbet, E. G., and Fowler, C. M. R., 1978. The Mid-Atlantic Ridge at 37°N. and 45°N. and some geophysical and petrological constraints. *Geophys. J. R. Astron. Soc.*, 54:631–660.

O'Hara, M. J., 1977. Geochemical evolution during fractional crystallization of a periodically refilled magma chamber. *Nature*, 266:503–507.

O'Hara, M. J., and Mathews, R. E., 1981. Geochemical evolution in an advancing, periodically replenished, periodically tapped, continuously fractionated magma chamber. *J. Geol. Soc. Lond.*, 138: 237–277.

Rhodes, J. M., Blanchard, D. P., Rodgers, K. V., et al., 1976. Petrology and chemistry of basalts from the Nazca Plate: Part 2—Major and trace element chemistry. *In* Yeats, R. S, Hart, S. R., et al., *Init. Repts. DSDP*, 34: Washington (U.S. Govt. Printing Office), 239–244.

Schmincke, H.-U., 1967. Fused tuff and peperites in south-central Washington. *Geol. Soc. Am. Bull.*, 78:319–330.

Sleep, N. H., 1975. Formation of ocean crust: Some thermal constraints. *J. Geophys. Res.*, 80:4037–4042.

_____, 1978. Thermal structure and kinematics of mid-ocean ridge axes: Some implications to basaltic volcanism. *Geophys. Res. Lett.*, 5:426–428.

Sparks, R. S. J., Meyer, P., and Sigurdsson, H., 1980. Density variation amongst mid-ocean basalts: Implications for magma mixing and the scarcity of primitive lavas. *Earth Planet. Sci. Lett.*, 46:419–430.

Stolper, E., and Walker, D., 1980. Melt density and the average composition of basalt, *Contrib. Mineral. Petrol.*, 74:7–12.

Talwani, M., Windisch, C. C., and Langseth, M. G., Jr., 1971. Reykjanes Ridge crest: A detailed geophysical study. *J. Geophys. Res.*, 76:473–517.

Tapponier, P., and Francheteau, J., 1978. Necking of the lithosphere and the mechanisms of slowly accreting plate boundaries. *J. Geophys. Res.*, 83:3955–3970.